J. Meas. Sci. Instrum., 2025, 16(3): 425-434. http://jmsi.publish.founderss.cn/
DOI: 10.62756/jmsi.1674-8042.2025041 jmsi@nuc.edu.cn

High-performance 2D/3D perovskite solar cells fabricated by in-situ blade-coating with low-volatility co-solvents

LIU Meihong[1], HAO Yafeng[1], MA Fupeng[1], ZHU Pu[1], WU Huijia[1], LI Ziwei[1], NIU Wenyu[1], HUANG Yujie[1], HUANGFU Guitian[2], LI Junye[2], LI Tengteng[1*], ZHANG Longlong[3*], LEI Cheng[1*], LIANG Ting[1]

1.State Key Laboratory of Extreme Environment Optoelectronic Dynamic Measurement Technology and Instrument, North University of China, Taiyuan 030051;

2. Shanxi Zhonghaiwei Rail Transit Engineering Co., Ltd., Taiyuan 030032;

3. State Key Laboratory of Solar Activity and Space Weather, National Space Science Center, Chinese Academy of Sciences, Beijing 100190

***Corresponding author:** LI Tengteng (litengteng@nuc.edu.cn); ZHANG Longlong (zhanglonglong@nssc.ac.cn); LEI Cheng (leicheng@nuc.edu.cn)

Received: August 20, 2025 **Revised:** September 12, 2025 **Accepted:** September 14, 2025

Abstract: Perovskite solar cells (PSCs) incorporating 2D/3D heterostructures have exhibited remarkable improvements in both power conversion efficiency and operational stability. Nevertheless, the prevalent spin-coating fabrication technique presents formidable challenges for scalable manufacturing processes. Herein, we present a blade-coating compatible methodology for fabricating high-performance 2D/3D PSCs utilizing a low-volatility t-amyl alcohol (t-AmOH) -dimethylformamide (DMF) mixed solvent system. Through systematic materials characterization and comprehensive device performance analysis, we demonstrate that this approach facilitates uniform spatial distribution of butylammonium iodide (BAI) organic spacers, thereby promoting the formation of a high-quality 2D/3D perovskite architecture characterized by enhanced crystallinity and substantially reduced defect density. The optimized device achieves a champion power conversion efficiency of 22.25% while demonstrating exceptional operational stability, retaining 83% of its initial performance after prolonged exposure under ambient conditions (45% relative humidity) for 1 000 h.

Key words: perovskite solar cells; 2D/3D heterostructures; blade-coating; interface passivation; scalable fabrication

0 Introduction

Perovskite solar cells (PSCs) have emerged as a highly competitive next-generation photovoltaic technology due to their exceptional optoelectronic properties, low fabrication costs, and rapidly improving power conversion efficiencies. Notably, the blade-coating fabrication technique enables scalable production of large-area PSCs, positioning this technology with substantial market potential across diverse application domains including mobile power systems, information electronics, high-altitude platforms, portable electronic devices, wearable technologies, intelligent transportation infrastructure, and building-integrated photovoltaic solutions[1,2]. Consequently, blade-coated PSCs have garnered significant research attention within the scientific community. Over the past decade, blade-coating methodologies for PSCs have undergone rapid advancement, with state-of-the-art blade-coated PSCs achieving certified power conversion efficiencies (PCEs) exceeding 24%[3-7]. Nevertheless, substantial challenges persist in realizing scalable manufacturing, particularly concerning device stability under operational conditions. The primary extrinsic factors contributing to performance degradation in PSCs encompass environmental humidity, thermal exposure, atmospheric oxygen, and light irradiation, among which moisture ingress represents the most critical degradation pathway[8].

To address the critical challenge of moisture-induced instability in PSCs, researchers have extensively explored multifaceted strategies, particularly focusing on blade-coating hydrophobic interfacial modification materials at functional layer interfaces. Furthermore, Lin et al.[9] developed an advanced dual interfacial modification strategy employing ethanolamine (EA) in synergistic combination with [2-(9H-carbazol-9-yl) ethyl] phosphonic acid (2PACz) for PSCs, wherein the complementary chemical structures of EA and 2PACz enabled synergistic passivation

effects that enhanced the photostability of perovskite thin films, consequently leading to significantly improved device stability. Although these pioneering approaches have demonstrably enhanced PSC stability, the intrinsic hydrophilic nature and inherent chemical instability of perovskite materials remain fundamental challenges that continue to impede the realization of long-term operational stability required for commercial applications. Fundamentally addressing this critical issue necessitates enhancing the intrinsic hydrophobicity of perovskite materials, which would provide a robust and comprehensive solution to the pervasive moisture instability problem plaguing PSCs[10-12]. Constructing a 2D/3D perovskite heterostructure at the interface between the perovskite active layer and charge transport layers represents an optimized architectural design, as the long organic chains inherent in 2D perovskites substantially enhance material hydrophobicity while maintaining 3D perovskite as the primary electronic framework ensures optimal carrier transport characteristics. Sidhik et al.[13] reported an innovative solution engineering methodology for fabricating 2D/3D perovskite heterojunctions, enabling the controlled deposition of 2D perovskites with thicknesses exceeding 50 nm while preserving exceptional phase purity and uniformity, and utilizing a 2D/3D perovskite heterojunction as the photoactive layer, their device architecture achieved outstanding performance metrics including a certified PCE of 24.5% and remarkable T_{99} operational stability exceeding 2 000 h. Niu et al.[14] further advanced this field through the development of a series of diammonium spacers specifically engineered for constructing ionic 2D/3D perovskite heterostructures, among which the 2D/3D device based on 2, 2-(ethylenedioxy) bis (ethylammonium) achieved an impressive PCE of 22.6% coupled with exceptional environmental stability, thereby highlighting the transformative potential of spacer chemistry design for high-performance 2D/3D PSCs. However, it is important to note that all previously reported 2D/3D perovskite architectures were fabricated exclusively using the spin-coating process, whereas large-area blade-coating has emerged as an essential manufacturing pathway for the industrialization of perovskite solar cells[15,16]. Consequently, the adaptation of 2D/3D perovskite fabrication to blade-coating processes remains insufficiently developed, with one of the primary technical challenges stemming from the rapid evaporation kinetics of highly volatile, low-boiling-point solvents such as isopropanol (IPA) typically employed to dissolve 2D perovskite organic ammonium salts, which leads to non-uniform distribution of the 2D perovskite organic ammonium salts at the active layer interface and significant difficulties in forming high-quality 2D/3D perovskite structures during the blade-coating process[17-20]. Therefore, the development of blade-coating methodologies for constructing high-quality 2D/3D perovskite structures holds substantial scientific significance and represents a critical frontier in advancing scalable PSC manufacturing technologies.

Herein, we present an innovative blade-coating methodology for fabricating high-performance 2D/3D PSCs through a strategically engineered low-volatility mixed solvent system, specifically utilizing tertiary amyl alcohol (t-AmOH) with inherently low volatility and dimethylformamide (DMF) as co-solvents, in conjunction with butylammonium iodide as the organic spacer solute, to enable controlled in-situ growth of 2D/3D perovskite heterostructures during the blade-coating process. This approach leverages the distinct physicochemical properties of the solvent system, wherein the reduced volatility of t-AmOH facilitates uniform spatial distribution and gradual deposition of butylammonium iodide atop the perovskite active layer, thereby promoting homogeneous interfacial integration, while DMF simultaneously accelerates Ostwald ripening kinetics to enhance the crystallization quality of the 2D/3D perovskite architecture and optimize charge carrier transport characteristics at the heterointerface. The resultant blade-coated 2D/3D PSCs demonstrate exceptional photovoltaic performance, achieving a PCE of up to 22.25%, which represents a substantial improvement over conventional device architectures. Furthermore, the intrinsic hydrophobic nature of the engineered 2D/3D perovskite structure confers enhanced environmental stability, enabling the fabricated devices to retain over 80% of their initial efficiency after prolonged storage under ambient atmospheric conditions (~45% relative humidity) for 1 000 h. We posit that this work establishes a robust technical paradigm for blade-coating fabrication of high-performance 2D/3D perovskite solar cells, offering significant potential for scalable manufacturing of stable photovoltaic devices.

1 Experiment

1.1 Materials

Lead iodide (PbI_2), formamidinium iodide (FAI), methylammonium iodide (MAI), methylammonium chloride (MACl), butylammonium iodide (BAI), bathocuproine (BCP), and fullerene (C_{60}) were purchased from Xi'an Yuri Solar Co., Ltd. Poly-4PACZ was

obtained from Wuhu Weiran New Energy Materials Technology Co., Ltd. All solvents, including t-AmOH, isopropanol, chlorobenzene and DMF were sourced from Sigma-Aldrich.

1.2 Device fabrication

The perovskite precursor was formulated by dissolving PbI_2 (1.2 mmol), FAI (0.84 mmol), and MAI (0.3 mmol) in anhydrous DMF (1 mL). Prior to device fabrication, the ITO-coated glass substrates were thoroughly cleaned through sequential ultrasonication in acetone and isopropanol (10 min for each solvent) followed by nitrogen blow-drying. The hole transport layer (HTL) solution was prepared by dissolving 5 mg of Poly-4PACZ in a mixed solvent system consisting of 600 μL chloroform and 400 μL methanol. A 20 μL aliquot of this solution was then blade-coated onto the pre-cleaned ITO substrates, which were subsequently annealed immediately on a hotplate at 100 ℃ for 10 min to ensure proper film formation and solvent removal. Immediately following the HTL deposition, 20 μL of the perovskite precursor solution was blade-coated onto the Poly-4PACZ-coated ITO substrate, followed by thermal annealing at 150 ℃ for 30 min to facilitate complete crystallization of the perovskite active layer. The BAI passivation layer was subsequently deposited using two distinct blade-coating methods to construct the 2D/3D perovskite heterostructure: a solution of BAI (4 mg·mL^{-1} in IPA) was prepared, and 20 μL was blade-coated onto the perovskite film; BAI (4 mg·mL^{-1}) was dissolved in t-AmOH with varying DMF volume ratios, and 20 μL of the solution was blade-coated under identical conditions. The device fabrication was completed by thermally evaporating a multilayer electrode structure under high vacuum ($<5\times10^{-4}$ Pa), beginning with a precisely controlled 2 nm BCP (bathocuproine) buffer layer deposited at 0.2 Å·s^{-1} to minimize interfacial recombination. This was followed by sequential deposition of a 25 nm C_{60} electron transport layer at 0.5 Å·s^{-1} for optimal charge extraction and a 100 nm Ag top electrode at 1.0 Å·s^{-1}.

1.3 Characterizations

The current density-voltage (J-V) characteristics and maximum power point (MPP) tracking were performed under standard AM 1.5 G illumination (100 mW·cm^{-2}) using an ABET SUN 3000 solar simulator coupled with a Keithley 2400 source measurement unit, with light intensity calibrated using a reference silicon photodiode (ABET Technology). External quantum efficiency (EQE) measurements were conducted with a Newport QE-PV-SI system incorporating a monochromator and source meter. Crystallographic analysis was performed using a Rigaku SmartLab 3000 X-ray diffractometer. Microstructural characterization was carried out using a JEOL JSM-6340 scanning electron microscope.

2 Results and discussion

To systematically investigate the effects of the low-volatility mixed solvent system on the growth morphology and crystalline quality of 2D/3D perovskite films, we fabricated ITO/ Self-assembled monolayer/perovskite stacked structures via blade coating for comprehensive characterization, with the resulting perovskite films prepared using different processing methods comprehensively analyzed through scanning electron microscopy (SEM) as presented in Fig.1(a) — (c). The standard perovskite film (without any post-treatment) exhibits numerous PbI_2 crystallites and relatively small grain sizes, whereas the perovskite film modified with a BAI layer (dissolved in isopropyl alcohol, denoted as BAI-IPA) fabricated by blade-coating atop the standard perovskite film demonstrates complete disappearance of PbI_2 crystallites due to Lewis acid-base coordination between BAI and PbI_2, leading to the formation of 2D perovskite phases; however, the BAI-IPA film shows considerable surface roughness resulting from the high volatility of IPA which causes rapid solvent evaporation during the coating process, leading to non-uniform BAI distribution and consequently uneven 2D perovskite coverage after annealing. In contrast, the 2D/3D perovskite film prepared using the low-volatility mixed solvent system (denoted as BAI-t-AmOH-DMF with 0.8% DMF by volume) exhibits exceptionally smooth and uniform morphology, as the low volatility of t-AmOH enables more homogeneous BAI distribution during the coating process, thereby facilitating optimal interfacial contact with the upper charge transport layer and significantly reducing interfacial defect density. Furthermore, we observe significantly enlarged perovskite grains in the BAI-t-AmOH-DMF film, which can be attributed to trace DMF promoting grain coalescence between 3D and 2D perovskite phases through Ostwald ripening, a process where smaller grains merge and grow into larger crystalline structures. Consequently, the BAI-t-AmOH-DMF film exhibits superior crystallinity and flatter surface morphology, as corroborated by atomic force microscopy (AFM) measurements presented in Fig.1(d) — (f), with RMS roughness values quantified at 29 nm for the control film, 25 nm for the BAI-IPA film, and 22 nm for the BAI-t-AmOH-DMF film, while XRD analysis

reveals significantly stronger perovskite diffraction peaks for the BAI-t-AmOH-DMF film compared to the other two samples. These comprehensive morphological and crystallographic characterization results demonstrate that the t-AmOH-DMF mixed solvent system simultaneously enables uniform BAI distribution across the underlying perovskite layer through minimized solvent evaporation during blade-coating facilitated by the low volatility of t-AmOH and maintains the perovskite surface in an optimally reactive state through the controlled partial dissolution effect from trace DMF, thereby promoting complete conversion of PbI_2 and facilitating Ostwald ripening to form large-grained 2D/3D perovskite structures with enhanced crystallinity as illustrated in Fig. 1(g), ultimately indicating that the BAI-t-AmOH-DMF film possesses superior charge transport properties and lower defect density based on the observed morphological and crystallographic improvements.

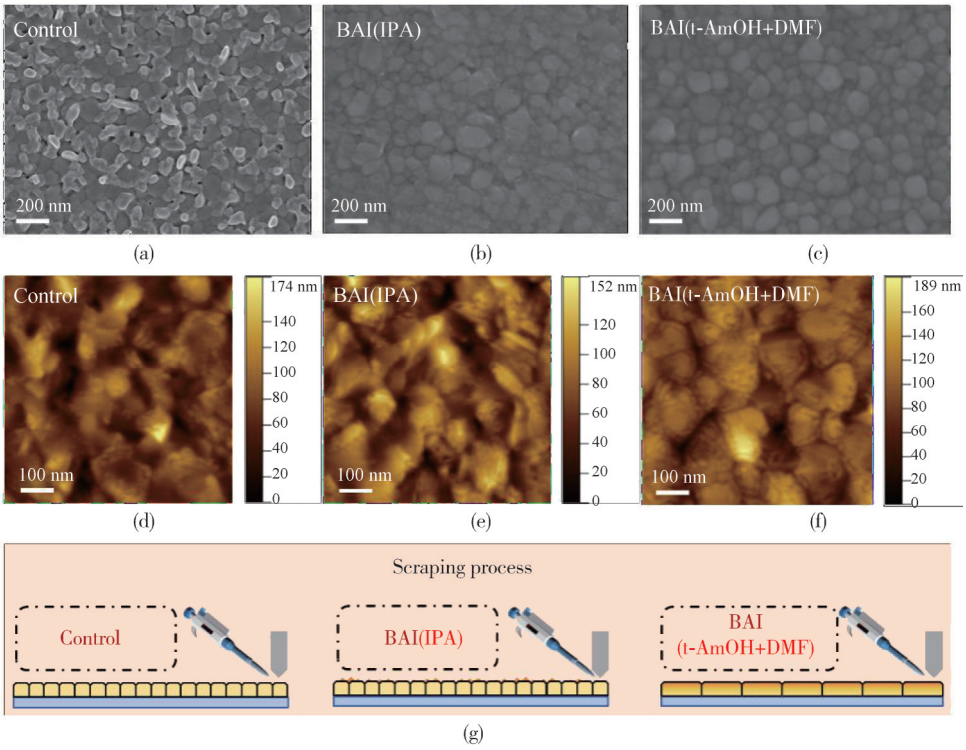

Fig. 1 SEM images of (a) standard perovskite film, (b) BAI-IPA perovskite film, and (c) BAI-t-AmOH-DMF perovskite film, respectively; (d) Atomic force microscopy (AFM) topographic images of standard perovskite film, (e) BAI-IPA perovskite film, and (f) BAI-t-AmOH-DMF perovskite film, respectively; and (g) Schematic illustration of perovskite film growth under different processing conditions.

X-Ray diffraction (XRD) characterization further corroborates these findings, revealing that the BAI-t-AmOH-DMF film exhibits the weakest PbI_2 diffraction peaks alongside the most intense perovskite signals (Fig. 2), a distinct crystallographic evolution demonstrating that the t-AmOH-DMF solvent system simultaneously facilitates complete conversion of residual PbI_2 through enhanced reaction kinetics with BAI and promotes Ostwald ripening-mediated growth of larger 2D/3D perovskite grains. The suppressed PbI_2 signatures confirm efficient consumption of lead iodide on the film surface during the phase transformation process, while the sharpened perovskite peaks reflect improved crystallinity with preferred orientation.

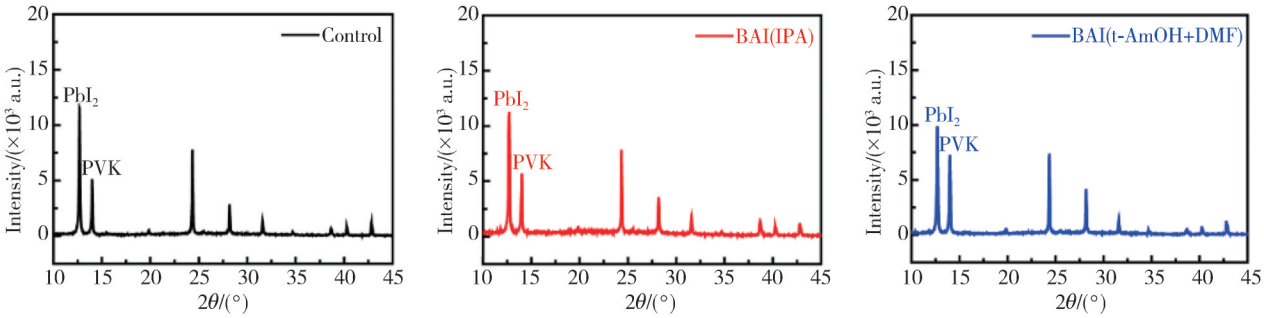

Fig. 2 XRD results for each kind of perovskite films.

To validate our hypothesis, we conducted steady-state photoluminescence (PL) measurements on perovskite films fabricated using different methods (Fig.3), with the BAI-t-AmOH-DMF films grown on glass substrates (without hole transport layers) exhibiting the strongest PL intensity followed by BAI-IPA and control films (Fig. 3(a)), a result indicating that the BAI-t-AmOH-DMF films possess the highest crystalline quality characterized by fewer defects and lower non-radiative recombination rates, which leads to enhanced PL emission[21-23]. When measured in complete device stacks (with hole transport layers and blade-coated electron transport layers), the BAI-t-AmOH-DMF films demonstrated the most efficient PL quenching while BAI-IPA and control films showed relatively weaker quenching effects (Fig. 3(b)), a phenomenon attributable to significantly reduced interfacial defects that facilitate faster charge transfer and improved interfacial contact quality resulting from the ultra-smooth surface morphology as evidenced by AFM characterization[24,25], with the superior interfacial properties of BAI-t-AmOH-DMF films enabling more efficient charge extraction at the transport layer interfaces.

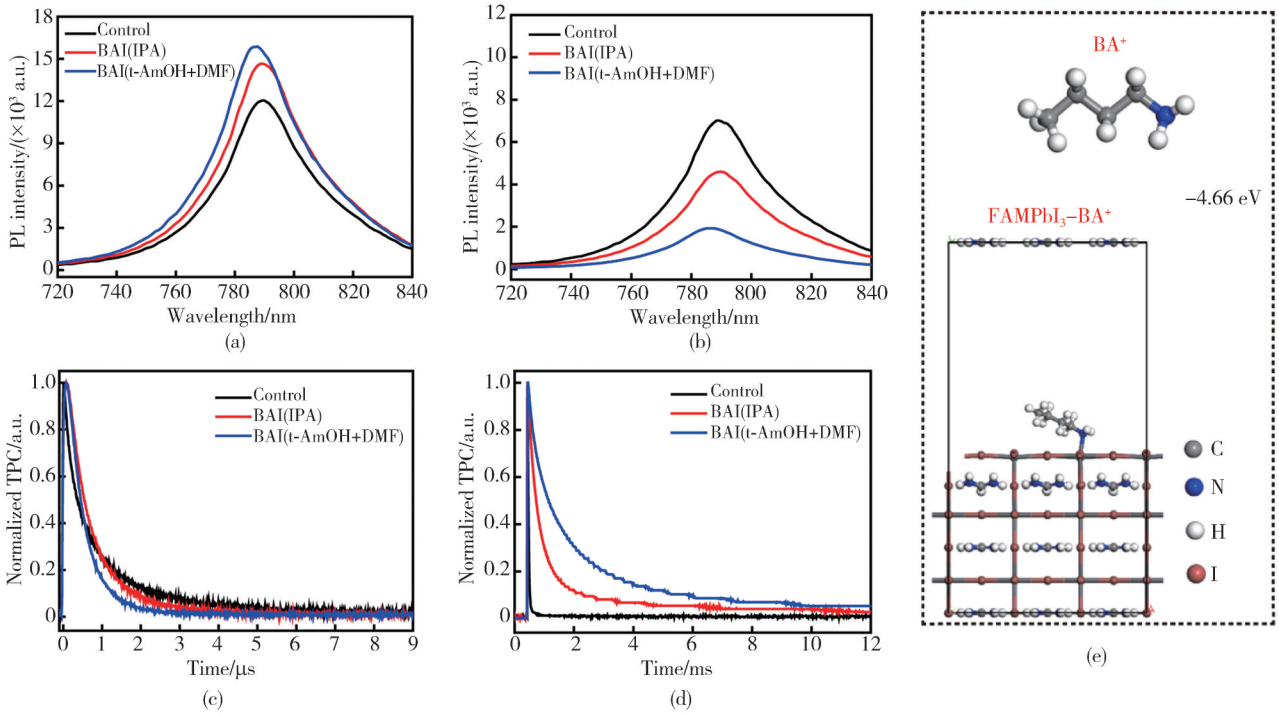

Fig. 3 Results of steady-state PL measurements on perovskite films fabricated using different methods. (a) PL spectra of glass/perovskite films; (b) PL spectra of ITO/HTL/perovskite/ETL films; (c) Transient photocurrent measurements of different perovskite films; (d) Transient photovoltage measurements of different perovskite films; (e) Formation energy calculations of perovskite-BAI.

These PL results provide compelling evidence supporting our previous conclusions regarding the enhanced film quality and superior interfacial characteristics achieved through the t-AmOH-DMF solvent engineering approach, as the combination of improved bulk film properties and optimized interfacial contact contributes to the observed performance enhancement in photovoltaic devices, and moreover, we observed a distinct blue shift in the PL emission peak of the BAI-t-AmOH-DMF film compared to both the BAI-IPA and control films (Fig.3(a), (b)), a spectral shift providing further evidence for the significant reduction of defect states in the BAI-t-AmOH-DMF film[26,27].

Transient photocurrent (TPC) and photovoltage (TPV) decay measurements provided further verification of our conclusions, with the fitted transient photocurrent decay time of the BAI-t-AmOH-DMF device (0.479 μs) significantly shorter than those of the BAI-IPA (0.651 μs) and control devices (0.788 μs) (Fig. 3(c)), while conversely the transient photovoltage decay times exhibited an opposite trend as the BAI-t-AmOH-DMF device demonstrated the longest decay time (1.117 ms) followed by BAI-IPA (0.717 ms) and control devices (0.025 ms) (Fig.3(d)). The shorter photocurrent decay time indicates faster charge carrier transport, consistent with the improved crystallinity and reduced trap states observed in previous characterizations[28,29], whereas the prolonged photovoltage decay time suggests significantly suppressed non-radiative recombination during charge transport, which aligns perfectly with the PL quenching behavior and blue shift

observations[30,31]. The excellent agreement between transient optoelectronic measurements and steady-state PL characterization provides compelling evidence for the superior charge dynamics in our optimized 2D/3D perovskite films, as the synergistic improvement in both charge transport and recombination properties explains the remarkable device performance enhancement achieved through the t-AmOH-DMF solvent engineering approach. We propose that under the effect of the t-AmOH-DMF mixed solvent system, BAI can not only form a 2D perovskite layer on the surface of control films but also interact with 3D perovskite to passivate defects, thereby reducing the defect density at film interfaces, a conclusion strongly supported by first-principles calculations revealing a negative formation energy of -4.66 eV for the BAI-FAMAPbI$_3$ system, with the thermodynamically favorable negative value indicating a stable interaction between these components and confirming their effective defect-passivation capability (Fig.3(e)).

As is well known, in addition to passivating interface defects, a crucial role of 2D/3D perovskite structures is to enhance the hydrophobicity of perovskite films and improve their stability under high-humidity conditions, which we systematically investigated through water contact angle measurements on different perovskite films as shown in Fig.4.

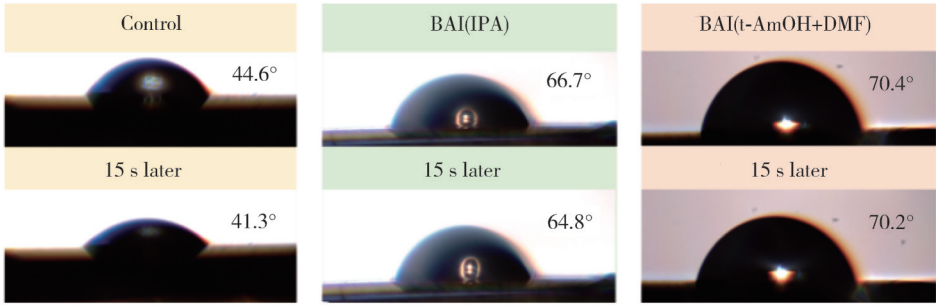

Fig. 4 Water contact angle measurements of perovskite films

The control film exhibited an initial water contact angle of 44.6° that decreased to 41.3° after 15 s, while the BAI-IPA film demonstrated a higher initial contact angle of 66.7° declining to 64.8° after the same duration, and notably the BAI-t-AmOH-DMF film showed the highest initial contact angle of 70.4° with only a minimal reduction to 70.2° after 15 s, resulting in percentage decreases in contact angle calculated as 7.4% for the control film, 2.8% for the BAI-IPA film, and merely 0.3% for the BAI-t-AmOH-DMF film. Compared to the control film, both BAI-IPA and BAI-t-AmOH-DMF films demonstrate significantly larger initial water contact angles, an improvement attributable to the formation of 2D/3D perovskite structures where the BA^+ organic long chains effectively enhance surface hydrophobicity[32], and the smaller reduction in water contact angle observed in these films further confirms their superior and more stable hydrophobic properties, with the BAI-t-AmOH-DMF film exhibiting the smallest water contact angle reduction because the uniformly distributed BAI forms an equally homogeneous 2D/3D structure resulting in enhanced structural stability and consequently optimal moisture resistance, a finding that is fully consistent with our previous conclusions.

The above characterization results demonstrate that the BAI-t-AmOH-DMF interface modification process can significantly improve both the crystalline quality and stability of 2D/3D perovskite films, and to further investigate the impact of different film fabrication methods on device performance we fabricated ITO/Poly-4PACZ/Perovskite/C60/ BCP solar cells with the device structure shown in Fig. 5(a), as summarized in Table 1, where the photovoltaic parameters were statistically analyzed using 30 devices for each group with the performance distribution shown in Fig. 6. The BAI-t-AmOH-DMF modified devices achieved an average PCE of 21.19% with a champion efficiency of 22.25%, substantially outperforming both the control devices (average PCE: 18.88%, champion: 19.59%) and BAI-IPA treated devices (average PCE: 19.91%, champion: 20.73%), and a detailed analysis of the photovoltaic parameters reveals that the performance enhancement of BAI-t-AmOH-DMF devices compared to control and BAI-IPA devices primarily originates from significant improvements in both open-circuit voltage (V_{OC}) and fill factor (FF), an improvement mechanism that can be attributed to the optimized charge transport layer interfaces and superior crystalline quality achieved in BAI-t-AmOH-DMF devices, as these structural advantages effectively suppress non-radiative carrier recombination, a critical factor directly governing V_{OC} and FF characteristics in perovskite solar cells[33-35], consequently the BAI-t-AmOH-DMF devices

demonstrate substantially enhanced photovoltaic performance.

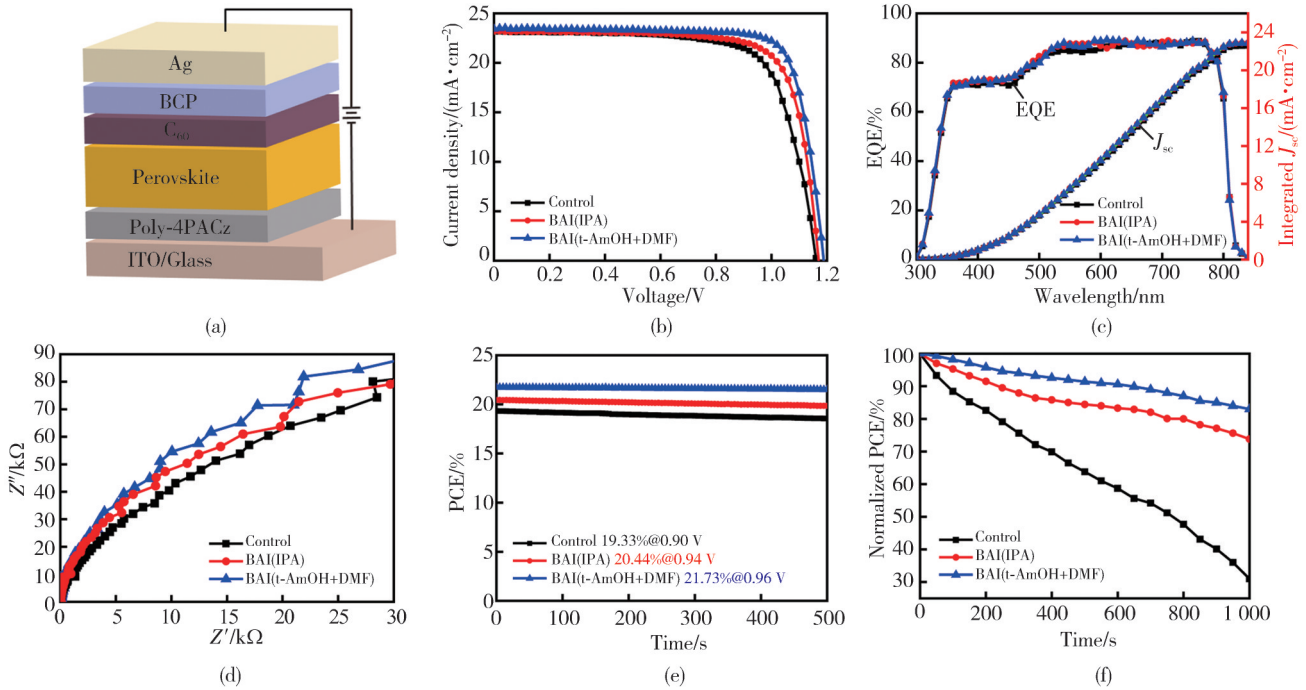

Fig. 5 Impact of different film fabrication methods on device performance. (a) Device architecture diagram; (b) J-V characteristics of champion device; (c) EQE measurements and short-circuit current densities of different devices; (d) Impedance spectra of different devices; (e) MPP tracking of different devices; and (f) Environmental stability tests of different devices.

Table 1 Photovoltaic performance of different PSCs. The data were obtained based on 30 cells for each condition

Sample	J_{sc}/(mA•cm^{-2})	V_{oc}/V	F_F/%	Average PCE/%	Best PCE/%
Control	22.72±0.43	1.150±0.008	72.25±0.77	18.88±0.45	19.59
BAI-IPA	22.63±0.42	1.164±0.006	75.60±0.47	19.91±0.46	20.73
BAI-t-AmOH-DMF	22.82±0.42	1.175±0.008	79.03±0.54	21.19±0.53	22.25

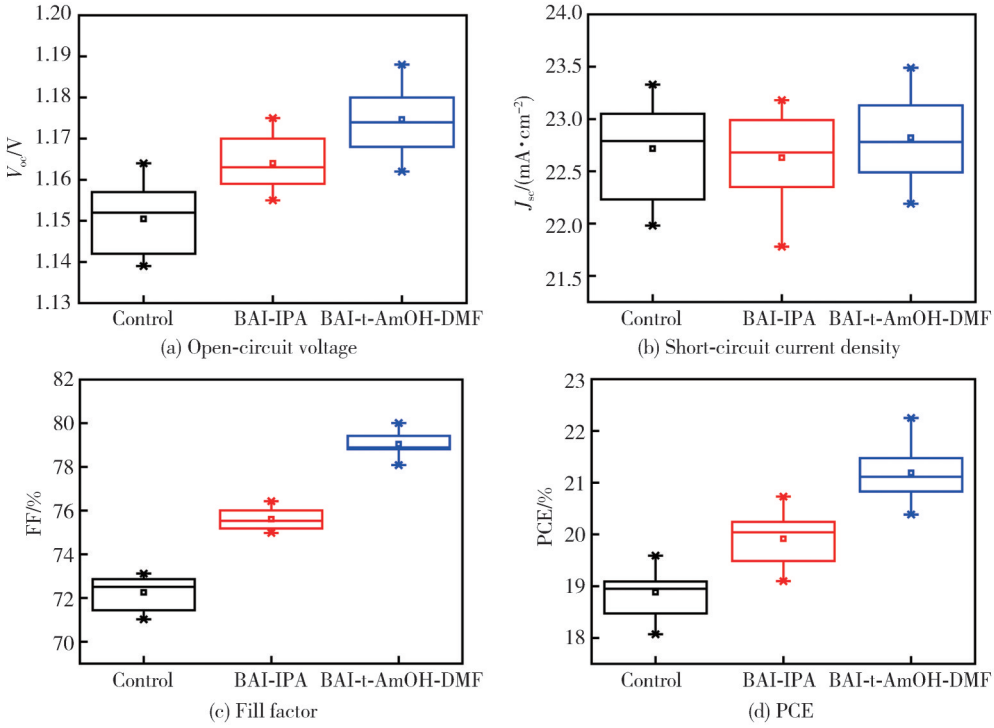

Fig. 6 Performance statistical distributions of different devices

Fig. 5(b) presents the current density-voltage (J-V) characteristics of champion devices across different categories, with the BAI-t-AmOH-DMF device achieving a peak PCE of 22.25% (V_{OC}=1.188 V, J_{SC}=23.45 mA·cm^{-2}, and F_F=79.85%), while in comparison the control and BAI-IPA devices exhibited inferior performance parameters, with the control device showing a PCE of 19.59% (V_{OC}=1.161 V, J_{SC}=23.16 mA·cm^{-2}, and F_F=72.84%) and the BAI-IPA device demonstrating a PCE of 20.73% (V_{OC}=1.172 V, J_{SC}=23.18 mA·cm^{-2}, F_F=76.43%). EQE measurements were conducted for current calibration, yielding integrated J_{SC} values of 22.89 mA·cm^{-2} for BAI-t-AmOH-DMF, 22.87 mA·cm^{-2} for BAI-IPA and 22.60 mA·cm^{-2} for control, all within 5% deviation from the J-V test results as shown in Fig. 5(c), and the optimization of device performance with different DMF volume ratios is shown in Table 2 and Fig. 7.

Table 2 Photovoltaic performance of BAI-t-AmOH-DMF photovoltaic devices with varying DMF volume ratios. The data were obtained based on 30 cells for each condition.

Sample	J_{sc}/(mA·cm^{-2})	V_{oc}/V	F_F/%	Average PCE/%	Best PCE/%
0.4% DMF	22.68±0.46	1.164±0.007	78.20±0.81	20.64±0.45	21.47
0.8% DMF	22.82±0.42	1.175±0.008	79.03±0.54	21.19±0.53	22.25
1.2% DMF	22.68±0.42	1.146±0.007	70.80±0.29	18.41±0.37	19.17

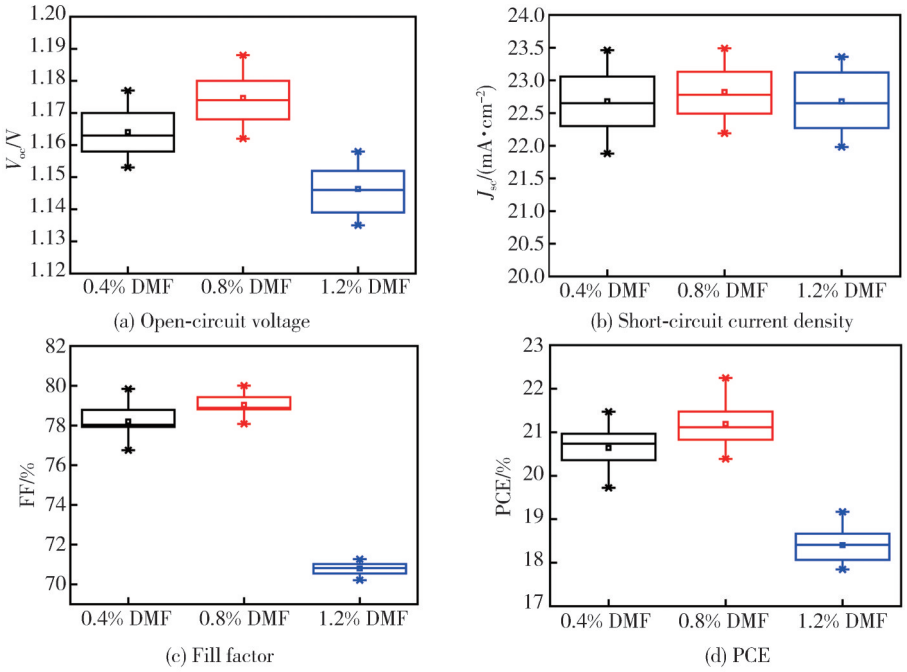

Fig. 7 Performance statistical distributions of BAI-t-AmOH-DMF photovoltaic devices with varying DMF volume ratios

Fig. 5(d) presents the Nyquist plots derived from electrochemical impedance spectroscopy measurements for control, BAI-IPA, and BAI-t-AmOH-DMF devices, with the BAI-t-AmOH-DMF device demonstrating markedly enhanced recombination resistance that directly evidences reduced defect-assisted recombination processes, a finding which aligns perfectly with our previous thin-film characterization results, and furthermore comprehensive stability evaluations through both maximum power point (MPP, 45% relative humidity) tracking and ambient aging tests (45% relative humidity) reveal the superior environmental stability of BAI-t-AmOH-DMF devices (Fig. 5(e)—(f)), as after 1 000 h of storage under ambient conditions these devices maintained 83% of their initial efficiency, significantly outperforming the BAI-IPA devices (73.8% retention) and control devices (31% retention), a pronounced stability enhancement that unambiguously confirms the critical role of the t-AmOH-DMF solvent system in optimizing both the interfacial properties and bulk stability of 2D/3D perovskite photovoltaic devices.

2 Conclusions

In this work, we developed an innovative BAI-t-AmOH-DMF interface modification strategy for fabricating high-performance 2D/3D PSCs through blade-coating, with systematic characterization confirming that the low-volatility t-AmOH-DMF mixed solvent facilitates uniform BAI distribution, thereby enabling the formation of a high-quality 2D/3D perovskite architecture characterized by enhanced

crystallinity and reduced defect density. Comparative analysis with control and BAI-IPA processed devices demonstrated that the BAI-t-AmOH-DMF modified devices exhibited significant photovoltaic performance improvements, attaining a champion PCE of 22.25% alongside remarkable operational stability, retaining 83% of their initial efficiency after 1 000 h of continuous exposure in ambient air (45% relative humidity). This work presents a novel and technically viable approach for blade-coating high-efficiency, stable 2D/3D perovskite solar cells, offering substantial potential for scalable manufacturing implementation.

Acknowledgement

This work was supported by ational Natural Science Foundation of China (Nos. 62405293, 62301509, 62304209), Key Research and Development Program of Shanxi Province (No. 202302030201001), Fundamental Research Program of Shanxi Province (Nos. 202303021212191, 202203021222079, 20210302123203, 202103021223185).

Declaration of conflicting interests

The authors have no conflict of interests related to this publication.

Reference

[1] SUN X, SHI W, LIU T, et al. Vapor-assisted surface reconstruction enables out-door-stable perovskite solar modules. Science, 2025, 388(6750): 957-963.

[2] YING Z Q, SU S Q, LI X, et al. Antisolvent seeding of self-assembled monolayers for flexible monolithic perovskite/Cu(In, Ga)Se_2 tandem solar cells. Nature Energy, 2025, 10(6): 737-749.

[3] National Renewable Energy Laboratory (NREL). (2023). Best research-cell efficiency chart. https://www.nrel.gov/pv/cell-efficiency.html.

[4] LI N X, TAO S X, CHEN Y H, et al. Cation and anion immobilization through chemical bonding enhancement with fluorides for stable halide perovskite solar cells. Nature Energy, 2019, 4(5): 408-415.

[5] PARK N G, ZHU K, Scalable fabrication and coating methods for perovskite solar cells and modules. Nature Reviews Materials, 2020, 5(5): 333-350.

[6] TROUGHTON J, BRYANT D, WOJCIECHOWSKI K, et al. Highly efficient, flexible, indium-free perovskite solar cells employing metallic substrates. Journal of Materials Chemistry A, 2015, 3(17): 9141-9145.

[7] DENG Y, PENG E, SHAO Y, et al. Scalable fabrication of efficient organolead trihalide perovskite solar cells with doctor-bladed active layers. Energy & Environmental Science, 2015, 8(5): 1544-1550.

[8] YANG J L, SIEMPELKAMP B D, LIU D Y, et al. Investigation of $CH_3NH_3PbI_3$ degradation rates and mechanisms in controlled humidity environments using in situ techniques. ACS Nano, 2015, 9(2): 1955-1963.

[9] LIN Y Z, CHEN B, ZHAO F W, et al. Matching charge extraction contact for wide-bandgap perovskite solar cells. Advanced Materials, 2017, 29(26): 1700607.

[10] WANG R, XUE J J, WANG K L, et al. Constructive molecular configurations for surface-defect passivation of perovskite photovoltaics. Science, 2019, 366(6472): 1509-1513.

[11] YANG S, WANG Y, LIU P R, et al. Functionalization of perovskite thin films with moisture-tolerant molecules. Nature Energy, 2016, 1: 15016.

[12] ZHANG T K, WANG F, KIM H B, et al. Ion-modulated radical doping of spiro-OMeTAD for more efficient and stable perovskite solar cells. Science, 2022, 377(6605): 495-501.

[13] SIDHIK S, WANG Y E, SIENA M D, A, et al. Deterministic fabrication of 3D/2D perovskite bilayer stacks for durable and efficient solar cells. Science 2022, 377(6613), 1425-1430.

[14] NIU T Q, LU J, MUNIR R, et al. Stable high-performance perovskite solar cells via grain boundary passivation. Advanced Materials, 2018, 30(16): 1706576.

[15] CHEN P, BAI Y, WANG S C, et al. In situ growth of 2D perovskite capping layer for stable and efficient perovskite solar cells. Advanced Functional Materials, 2018, 28(17): 1706923.

[16] YANG R, LI R, Z CAO Y, WEI Y, et al. Oriented quasi-2D perovskites for high performance optoelectronic devices. Advanced Materials, 2018, 30(5): 1804771.

[17] LI J B, MUNIR R, FAN Y Y, et al. Phase transition control for high performance blade-coated perovskite solar cells. Joule, 2018, 2(7): 1313-1330.

[18] YANG M J, LI Z, REESE M O, et al. Perovskite ink with wide processing window for scalable high-efficiency solar cells. Nature Energy, 2017, 2: 17038.

[19] DENG Y H, DONG Q F, BI C, et al. Air-stable, efficient mixed-cation perovskite solar cells with Cu electrode by scalable fabrication of active layer. Advanced Energy Materials, 2016, 6(11): 1600372.

[20] SUN X, ZHANG C F, CHANG J J, et al. Mixed-solvent-vapor annealing of perovskite for photovoltaic device efficiency enhancement. Nano Energy, 2016, 28: 417-425.

[21] TURREN-CRUZ S. H, HAGFELDT A, SALIBA M. Methylammonium-free, high-performance, and stable perovskite solar cells on a planar architecture. Science, 2018, 362(6413): 449-453.

[22] DONG Q F, FANG Y J, SHAO Y C, et al. Electron-hole diffusion lengths >175 μm in solution-grown CH3NH_3PbI_3 single crystals. Science, 2015, 347(6225): 967-970.

[23] DE QUILETTES D W, VORPAHL S M, STRANKS S D, et al. Impact of microstructure on local carrier lifetime in

perovskite solar cells. Science, 2015, 348(6235): 683-686.
[24] WU W Q, RUDD P N, NI Z, et al. Reducing surface halide deficiency for efficient and stable Iodide-based perovskite solar cells. Journal of the American Chemical Society, 2020, 142(8): 3989-3996.
[25] ABDI-JALEBI M, ANDAJI-GARMAROUDI Z, CACOVICH S, et al. Maximizing and stabilizing luminescence from halide perovskites with potassium passivation. Nature 2018, 555(7697): 497-501.
[26] BIRKHOLD S T, ZIMMERMANN E, KOLLEK T, et al. Impact of crystal surface on photoexcited states in organic-inorganic perovskites. Advanced Functional Materials, 2016, 27(6): 1604995.
[27] ZHENG X P, CHEN B, DAI J, et al. Defect passivation in hybrid perovskite solar cells using quaternary ammonium halide anions and cations. Nature Energy, 2017, 2: 17102.
[28] PENG J, CHEN Y, ZHENG K, et al. Insights into charge carrier dynamics in organo-metal halide perovskites: from neat films to solar cells. Chemial Society Reviews, 2017, 46(19): 5714-5729.
[29] JOHNSTON M B, HERZ L M. Hybrid perovskites for photovoltaics: Charge-carrier recombination, diffusion, and radiative efficiencies. Accounts of Chemical Research, 2016, 49(11): 146-154.
[30] NENON D P, CHRISTIANS J A, WHEELER L M, et al. Structural and chemical evolution of methylammonium lead halide perovskites during thermal processing from solution. Energy & Environmental Science, 2016, 9(6): 2072-2082.
[31] YUAN J, HAZARIKA A, ZHAO Q, et al. Metal halide perovskites in quantum dot solar cells: progress and prospects. Joule, 2020, 4(6): 1160-1185.
[32] GRANCINI G, ROLDÁN-CARMONA C, ZIMMERMANN I, et al. One-year stable perovskite solar cells by 2D/3D interface engineering. Nature Communications, 2017, 8: 15684.
[33] CORREA-BAENA J P, ABATE A, SALIBA M, et al. The rapid evolution of highly efficient perovskite solar cells. Energy & Environmental Science, 2017, 10(3): 710-727.
[34] JIANG Q, ZHAO Y, ZHANG X W, et al. Surface passivation of perovskite film for efficient solar cells. Nat. Photonics, 2019, 13(7): 460-466.
[35] MIN H, KIM M, LEE S U, et al. Efficient, stable solar cells by using inherent bandgap of α-phase formamidinium lead iodide. Science ,2019, 366(6466): 749-753.

基于低挥发性混合溶剂原位刮涂制备高性能2D/3D钙钛矿太阳电池

刘美宏[1], 郝亚峰[1], 马富鹏[1], 朱 璞[1], 武慧嘉[1], 李子唯[1], 牛文宇[1], 黄育杰[1], 皇甫贵田[2], 李俊叶[2], 李腾腾[1*], 张龙龙[3*], 雷 程[1*], 梁 庭[1]

1. 中北大学 极限环境光电动态测试技术与仪器全国重点实验室, 山西 太原 030051;
2. 山西中海威轨道交通工程有限公司, 山西 太原 030032;
3. 中国科学院国家空间科学中心 太阳活动与空间天气全国重点实验室, 北京 100190

摘 要： 二维/三维钙钛矿异质结构可有效提升钙钛矿太阳电池的光电转换效率和稳定性。然而，目前广泛采用的旋涂制备技术难以满足规模化生产需求。本研究提出了一种基于刮涂工艺的钙钛矿太阳电池制备方案，利用低挥发性叔戊醇-二甲基甲酰胺混合溶剂，成功制备出高性能二维/三维钙钛矿太阳电池。通过系统化的材料表征与全面的器件性能分析，我们证实该方法可实现丁基碘化铵衍生产物在钙钛矿薄膜表面的均匀分布，从而促进高质量二维/三维钙钛矿结构的形成，使其具有更高的钙钛矿晶体质量和更少的缺陷密度。经该工艺优化后的钙钛矿电池实现了22.25%的最高能量转换效率，并展现出卓越的稳定性：在环境条件（相对湿度45%）下持续运行1 000小时后，仍能保持初始性能的83%。

关键词： 钙钛矿太阳电池；二维/三维异形结构；刮涂法；界面钝化；产业化工艺

引用格式： LIU Meihong, HAO Yafeng, MA Fupeng, et al. High-performance 2D/3D perovskite solar cells fabricated by in-situ blade-coating with low-volatility co-solvents. Journal of Measurement Science and Instrumentation, 2025, 16(3): 425-434. DOI: 10.62756/jmsi.1674-8042.2025041